Non-galvanic Hydrogen Production Using High Steam Pressure Gradients

Sun-Ju Song* and Eric D. Wachsman
Department of Materials Science and Engineering, University of Florida, Gainesville, FL 32611, U.S.A.

(Received June 5, 2006; CL-060639; E-mail: song@anl.gov)

Equilibrium defect concentrations calculated by numerical modeling based on a point defect model showed that protons and electrons were predominant defects under reducing and high pH_2O conditions. Hydrogen permeation flux for 1 mm $SrCe_{0.95}Y_{0.05}O_{3-d}$ membranes was derived on the basis of chemical diffusion theory as functions of pO_2 and pH_2O. Hydrogen permeation flux keeps increasing with increasing water vapor pressure gradient with a reference to 10^{-6} atm of pH_2O.

Considerable attention in the development of an environmentally benign, high performance, inexpensive technology for separating hydrogen during industrial processes has motivated the research on hydrogen permeable membranes.[1–4] Among membrane materials, inorganic membranes are a candidate for non-galvanic hydrogen production due to their potential cost effectiveness, and higher tolerance to corrosive gas in extreme conditions. However, there are significant technical challenges including the development of membranes that can withstand sever operating conditions of elevated temperature and pressure.

Research to date[5–7] has focused on the effect of hydrogen potential gradients across membranes, but not much attention has been given to the high steam pressure gradient on membranes. Because it was thought that the maximum proton uptake might be limited by oxygen vacancies generated by doped acceptor in perovskite oxides,[8,9] however, the solubility of protons at high temperature increased with structural stability and packing density of the oxides.[10] It was also suggested that the water saturation limit is determined by the dopant distribution over the two cation sites and the dependence on oxygen relaxation around oxygen ion vacancies.[11] Furthermore, from the defect equilibrium diagram studies on proton-conducting perovskite oxides,[12,13] protons increases as $1/2$ power of pH_2O at low vapor pressure, and then increases as $1/4$ power of pH_2O at high vapor pressure.

Therefore, focus on high-steam pressure and temperature effect on membranes was given in this study. Numerical modeling was attempted to calculate the hydrogen permeation flux as a function of water vapor pressure across the inorganic membranes.

Among the many ABO_3-type perovskite oxide, Y-doped strontium cerate was selected as a model system because their thermodynamic equilibrium constant values were available.

In previous works,[14–16] we reported a complete model for the defect chemisty of Y-doped strontium cerate. By applying Poulson's method,[17] the concentration of each defect species was successfully calculated as functions of given thermodynamic conditions and flux equation was numerically solved with partial conductivities.

The chemical diffusion of protons and electrons may be described within the framework of chemical diffusion theory,[18] because transport of protons, oxygen ions, holes and electrons across the ceramic membrane is driven by concentration gradients. Assuming the local thermodynamic equilibria and an open circuit conditions, the hydrogen permeation flux equation may be derived as functions of pO_2 and pH_2O:

$$J_{H_2} = -\frac{1}{L}\left\{\frac{RT}{4F^2}\int_{P^{\prime}_{H_2O}}^{P^{\prime\prime}_{H_2O}} \sigma_t t_{H^+}(t_{O^{2-}} + t_e)\mathrm{d}\ln P_{H_2O} - \frac{RT}{8F^2}\int_{P^{\prime}_{O_2}}^{P^{\prime\prime}_{O_2}} \sigma_t t_{H^+} t_e \mathrm{d}\ln P_{O_2}\right\}, \quad (1)$$

where L is the membrane thickness (1-mm thick), σ_i represents the partial conductivity of species i, and t_i is the transference number of defect species i.

All of the equilibrium constants used for the simulation are experimentally determined values, except K_s. Because the concentration are expressed here in mole fraction, the factor (W_m/dA), where W_m is the molecular weight, d is the density of oxide, and A is Avogadro's number, is multiplied to the values of the equilibrium constant for consistent units (mole defect/formula unit mole).

The defect concentration profile as a function of pH_2O is shown in Figure 1. As expected from previous defect equilibrium studies, electrons are charge compensated by effective positive charge oxygen vacancies at low vapor pressure and by protons at high vapor pressure. As water vapor pressure increases, oxygen vacancy concentration decreases due to the proton incorporation reaction:

$$H_2O(g) + V_O^{\bullet\bullet} + O_O^x \rightarrow 2OH_O^{\bullet} \quad (2)$$

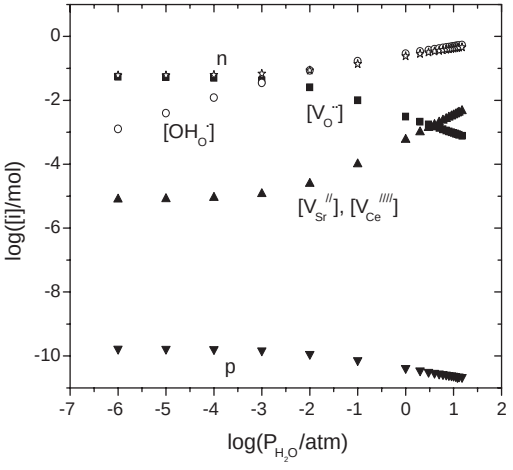

Figure 1. Defect concentrations of Y-doped $SrCeO_{3-d}$ as a function of water vapor pressure at 973 K.

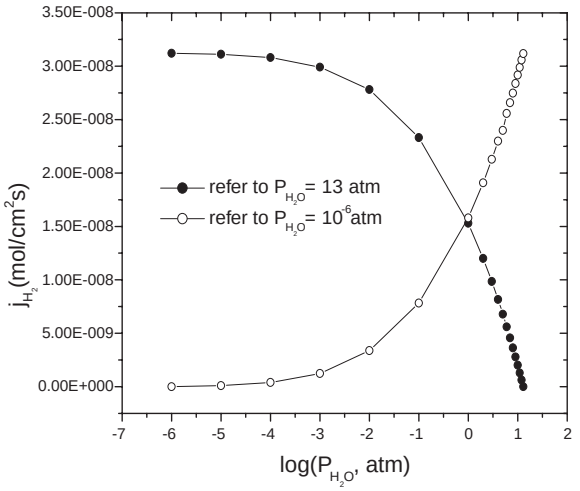

Figure 2. Numerically calculated hydrogen permeation fluxes at 973 K. Open circle: with the reference to fixed 10^{-6} atm of pH_2O. Closed circle: with the reference to fixed 13 atm of pH_2O.

Under oxidizing and high vapor pressure conditions, it also shows that proton incorporation exceeds oxygen vacancy concentration with increasing cation vacancy concentration. One may infer that proton incorporation can proceed without lattice oxygen vacancies and the effective negatively charged cation vacancies are compensated by positive-charged protons. Cation deficiency in doped strontium cerate could be explained by the fact that the three-valent yttrium dopant can substitute not only for the cerium site but also for the strontium site while strontium ions are segregated or vaporized as pointed out by other researchers.[19,20]

The integration of equation 1 requires information about partial conductivities as a function of hydrogen and oxygen activity. The partial conductivity may be calculated in terms of the product of the concentration and electrical mobility of the defect species at a given thermodynamic condition. The mobility for protons, oxygen vacancies, and holes are extracted from conductivity measurements,[21] $1.45 \cdot 10^{-5}$, $6.48 \cdot 10^{-6}$, and $4.11 \cdot 10^{-4}\,\mathrm{cm^2/V\,s}$ at 973 K, respectively by assuming that the defect's mobilities are independent of both hydrogen and oxygen activity.

The hydrogen permeation flux reaches a maximum ($3.1 \cdot 10^{-8}\,\mathrm{mol/cm^2\,s}$) with the reference to fixed 13 atm of pH_2O and becomes independent of the pH_2O on the water vapor lean side, as shown in Figure 2. In contrast, the hydrogen permeation flux keeps increasing with water vapor pressure with the reference to fixed 10^{-6} atm of pH_2O. Because it was reported that the hydrogen permeation flux is inversely proportional to membrane thickness down to several micrometer thickness,[22] significant increase in hydrogen permeation flux could be achieved by decreasing the membrane thickness.

With chemical diffusion theory as the basis, and a point defect model, we obtained hydrogen permeation fluxes by numerical modeling as a function of water vapor pressure. Focus was given to the effect of high steam pressure gradient on membranes. The result shows that a significant hydrogen permeation flux may be achieved under high water vapor pressure gradients.

This work was supported by NASA Glenn Research Center under grant NAG 3-2930.

References

1 H. Iwahara, T. Esaka, H. Uchida, N. Maeda, *Solid State Ionics* **1981**, *3–4*, 359.
2 H. Iwahara, T. Yajima, T. Hibino, H. Uchida, *J. Electrochem. Soc.* **1993**, *140*, 1687.
3 H. Iwahara, *Solid State Ionics* **1995**, *77*, 289.
4 S. Hamakawa, T. Hibino, H. Iwahara, *J. Electrochem. Soc.* **1994**, *141*, 1720.
5 S.-J. Song, T. H. Lee, E. D. Wachsman, L. Chen, S. E. Dorris, U. Balachandran, *J. Electrochem. Soc.* **2005**, *152*, J125.
6 X. Qi, Y. S. Lin, *Solid State Ionics* **2000**, *130*, 149.
7 S.-J. Song, E. D. Wachsman, J. Rode, S. E. Dorris, U. Balachandran, *Solid State Ionics* **2004**, *167*, 99.
8 T. Schober, J. Friedrich, *Solid Stat Ionics* **1999**, *125*, 319.
9 F. Krug, T. Schober, *Solid State Ionics* **1996**, *92*, 297.
10 Y. Larring, T. Norby, *Solid State Ionics* **1997**, *97*, 523.
11 K. D. Kreuer, T. Dippel, Y. M. Baikov, J. Maier, *Solid State Ionics* **1996**, *86–88*, 613.
12 N. Bonanos, *Solid State Ionics* **1992**, *53–56*, 967.
13 S.-J. Song, E. D. Wachsman, S. E. Dorris, U. Balachandran, *Solid State Ionics* **2002**, *149*, 1.
14 S.-J. Song, E. D. Wachsman, J. Rode, S. E. Dorris, U. Balachandran, *Solid State Ionics*, **2003**, *164*, 107.
15 S.-J. Song, E. D. Wachsman, J. Rhodes, H.-S. Yoon, K.-H. Lee, G. Zhang, S. E. Dorris, U. Balachandran, *J. Mater. Sci.* **2005**, *40*, 4061.
16 S.-J. Song, E. D. Wachsman, S. E. Dorris, U. Balachandran, *J. Electrochem. Soc.* **2003**, *150*, A1484.
17 F. W. Poulsen, *J. Solid State Chem.* **1999**, *143*, 115.
18 C. Wagner, *Prog. Solid State Chem.* **1975**, *10*, 3.
19 S. M. Haile, G. Staneff, F. H. Ryu, *J. Mater. Sci.* **2001**, *36*, 1149.
20 R. Glockner, M. S. Islam, T. Norby, *Solid State Ionics* **1999**, *122*, 145.
21 S.-J. Song, E. D. Wachsman, S. E. Dorris, U. Balachandran, *J. Electrochem. Soc.* **2003**, *150*, A790.
22 S. Hamakawa, L. Anwu, E. Iglesia, *Solid State Ionics* **2002**, *148*, 71.

Published on the web (Advance View) August 23, 2006; doi:10.1246/cl.2006.1068